


Spontaneous Frequency Shift and Phase Delay of Coupled Terahertz Radiation Mediated by the Josephson Plasmon in a Cuprate Superconductor

Ryota Kobayashi,^{1,†} Ken Hayama,^{1,†} Shuma Fujita,¹ Manabu Tsujimoto^{1,2,‡} and Itsuhiro Kakeya^{1,*}

¹*Department of Electronic Science and Engineering, Kyoto University, Kyotodaigaku Katsura, Nishikyo, Kyoto 615-8510, Japan*

²*Research Center for Emerging Computing Technologies, National Institute of Advanced Industrial Science and Technology (AIST), Central2, 1-1-1 Umezono, Tsukuba, Ibaraki 305-8568, Japan*

 (Received 4 October 2021; revised 12 March 2022; accepted 19 April 2022; published 25 May 2022)

We examine coupling interactions used to synchronize macroscopic Josephson oscillations induced in intrinsic Josephson-junction (IJJ) mesa stacks made of a Bi2212 single crystal. Synchronized radiations of terahertz electromagnetic (EM) waves are detected under common voltage and current bias operations of two connected mesas with close individual radiation frequencies, while uncoupled and bimodal radiations are frequently observed in two mesas with different individual radiation frequencies. Detailed observations of the polarizations of the EM waves emitted when two mesas are biased in parallel or series allow us to reveal the coupling matrix components, which include ratios of synchronized IJJs in the mesas and phase delay between the macroscopic Josephson oscillations. A frequency evolution of the phase delay implies that the coupling between the Josephson oscillations is mediated by the small amplitude Josephson plasmon inside the superconducting substrate. This finding stimulates systematic survey on polarization of EM wave emitted from synchronized multiple mesa devices in order to realize powerful terahertz emissions from superconductors.

DOI: [10.1103/PhysRevApplied.17.054043](https://doi.org/10.1103/PhysRevApplied.17.054043)

I. INTRODUCTION

Various phenomena attributed to couplings between Josephson junctions have been observed in cuprate superconductor single crystals, in which a strong modulation of order parameter along the c axis attributed to the layered crystal structure exists [1]. In such systems, known as intrinsic Josephson junctions (IJJs), the excitation of a Josephson plasma wave along the a - b plane [2,3] induces macroscopic current oscillations on the crystal surface owing to the interplay with the ac Josephson effect and their synchronous oscillations accompanied by the inductive and the capacitive couplings among stacked IJJs [4–7], which cause electromagnetic (EM) radiation into space [8–10]. Intensive research has been carried out on Josephson plasma emission (JPE) using mesa-structured devices formed from Bi₂Sr₂CaCu₂O_{8+δ} (Bi2212) single crystals [11–20], and further research on the possibility of a terahertz (THz) source have been

reported during this decade [21–33]. For the implementation of this JPE for a practical terahertz source, it is indispensable to manage the synchronous oscillations resulting in higher radiation power and controlled performances. However, the microscopic interaction between thousands of IJJs included in the mesa devices have not been fully revealed partly because of the lack of experimental results in a single-layer IJJ with the similar a - b plane geometry to existing JPE devices.

One of the straightforward strategies to increase the radiation intensity is to synchronize multiple mesas to emit radiation. As an initial attempt, when two mesas were connected in series, the coupled emission intensity was found to be higher than the sum of the individual intensities [34]. Next, for a device with up to three mesas connected in parallel, an intensity of 0.61 mW was achieved, which is roughly proportional to the square of the number of mesas to be synchronized, and it was concluded that the emission of the electric wave is a synchronous coherent radiation [35].

Very recently, the authors proposed a method for analyzing the synchronous phenomena with bases as polarizations of singly biased radiations and a coupling matrix between the Josephson plasma waves excited in the mesas from precise observations of the polarization of the radiated EM wave [36,37]. This method allows us to determine

*Corresponding author. kakeya@kuee.kyoto-u.ac.jp

†These authors contributed equally.

‡Faculty of Pure and Applied Sciences, University of Tsukuba, 1-1-1 Tennodai, Tsukuba, Ibaraki 305-8573, Japan

the contribution of each mesa to the synchronized emission under biasing multiple mesas. It is crucial to compare the emission features for parallel and series connections of a pair of mesas because the coupling matrix can be modified with the identical bases. However, there has been no report of investigations on the differences between them in an identical device. Regarding a radiating mesa in which a thousand stacked IJJs oscillate coherently as a macroscopic Josephson junction [38], the common voltage bias (CVB) produced by the parallel connection should induce synchronous oscillations between the macroscopic Josephson junctions, whereas the common current bias (CCB) produced by the series connection gives insights for the interplay between a few stacked IJJs [39–42].

In this paper, we discuss the difference in intermesa coupling when two of three mesas are operated either by CVB or CCB modes, based on the polarization observation of EM waves emitted from mesas in individual and coupled emission states. A CVB mode mostly generates a coupled emission with unimodal frequency spectrum, whereas a CCB mode tends to generate an uncoupled emission with bimodal frequency spectrum. The coupled emission state is a superposition of the individual emissions perturbed by the intermesa coupling. The coefficients of the linear combination with the bases of the individual oscillation states, which are chosen necessarily, compose the mesa interaction matrices, i.e., the states of the harmonically oscillating plasmons inside the superconducting substrate that are responsible for the interaction between the *non-linear* Josephson plasma oscillations in the mesas [43]. A systematic survey of the interaction matrix will lead to the development of powerful THz sources by controlling the mesa-to-mesa synchronization and will stimulate emergence of superconducting devices that enable THz quantum communication.

II. EXPERIMENT

In this study, we discuss EM wave radiations from three mesas (*B*, *C*, and *E*) formed on a Bi2212 single crystal grown by the floating zone method using photolithography and argon ion milling [19,24]. The device is shown in Fig. 1(a). The basic properties, such as the mesa shape, T_c , and current-voltage characteristics of the three mesas, are summarized in Appendix A. Parallel and series connections can simultaneously energize a pair of mesa structures connected by a Bi2212 substrate single crystal with CVB and CCB modes, respectively. For a CVB mode, the wires connected to the two mesas are short circuited at the outside of the cryostat, and a voltage is applied between the electrode and the substrate crystal, so that the same voltage is applied to the connected mesas, as shown in the right panel of Fig. 1(a). On the other hand for a CCB mode, a bias voltage is applied between the two mesas, so it is not ensured that the same voltage is applied to

each mesa. An EM wave emitted is detected by a silicon bolometer cooled by liquid helium [24], and the intensity is evaluated by the bolometer output voltage and the radiation frequency measured using a FTIR spectrometer with a pair of lamellar mirrors [15,44,45]. For the polarization evaluation, the Stokes polarization parameters (SPPs) are estimated from the transmitted intensity through a polarization analyzer combining a fixed linear polarizer and a rotating achromatic quarter-wave plate (QWP) [46] as described in Refs. [36,47,48].

III. RESULTS AND DISCUSSION

A. Current-voltage characteristics and emission intensity

Figure 1(b) shows the current-voltage-emission (I - V - E) characteristics of mesas *B* and *E* under CVB. This situation is represented by $B \parallel E$ hereinafter. In comparison to data for individual mesas *B* and *E* [Figs. 1(c) and 2 in Appendices], the current-voltage characteristics (IVC) for $B \parallel E$ is elongated twice with respect to the current, and the emission intensity indicates more complicated multimodal behavior as a function of the total bias current [Fig. 1(b), right panel]. First, the I - V curve for $B \parallel E$ with increasing bias is explained. Below 25 mA, both *B* and *E* are superconducting and their bias currents are equal. Between 25 and 50 mA, unequal currents flow in mesas *B* and *E* to keep CVB thus parts of IJJs of the mesas become resistive. In the E - I curve for $B \parallel E$, two intensity maxima are observed: a broad maximum at $I = 48$ mA, and a rather sharp maximum at $I = 26$ mA. The former current is slightly higher than the sum of the bias currents for the maximum emission intensity of both mesas *B* and *E* ($\simeq 22$ mA, commonly). Here, both mesas participate in the radiation. The latter current approximately correspond to the sum of the bias current for the maximum emission intensity of either mesa *B* or *E* and the current ($\simeq 3$ mA) for the same bias voltage region due to the multivalent IVC [15,19]. One mesa emits intensively with 22 mA, while the other does not under biasing at the same voltage. As listed in Table I, the maximum detected intensity P_{\max} for $B \parallel E$ is slightly smaller than the sum of P_{\max} 's for *B* and *E* and the second maximum intensity for $B \parallel E$ is very close to the P_{\max} for *B* or *E*. Thus, we interpret that for $B \parallel E$ both mesas *B* and *E* contribute to the emission above 40 mA while only either one contributes between 20 and 40 mA. The breakings of the I - V curve (at 40 and 18 mA) are attributed to the switchings of the internal synchronous phase dynamics of each mesas. This feature is consistent with a numerical calculation in a similar system consisting of two IJJ stacks connected in parallel [49]. In the subsequent discussion, therefore, spectra and polarization data above 40 mA for $B \parallel E$ are employed for comparison between simultaneous and individual emissions.

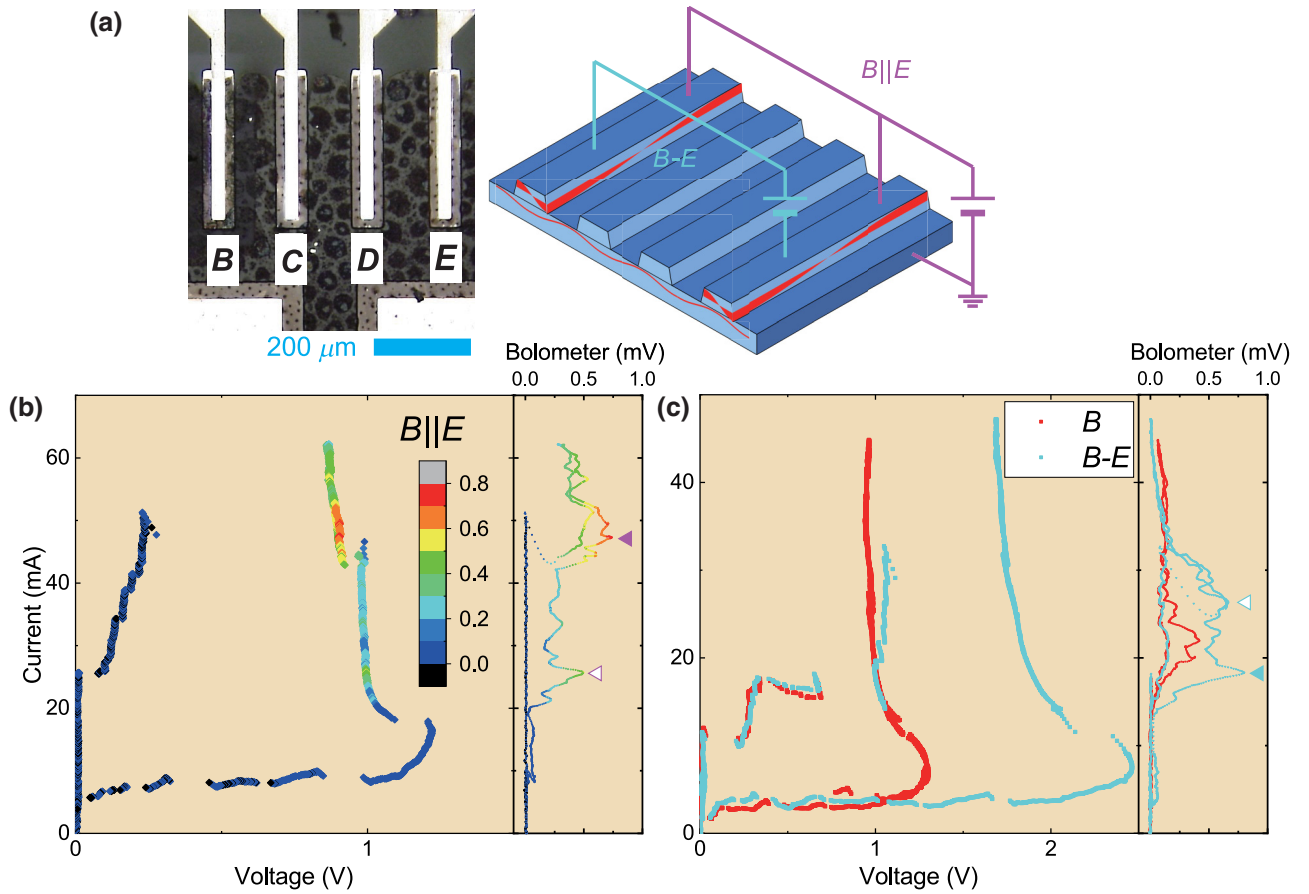


FIG. 1. (a) Microscope picture of the device (left) and a schematic drawing of the device and their connections for $B \parallel E$ (right, magenta) and $B-E$ (cyan). Properties of mesa D are not dealt with in this paper. Separations between mesas (d) are 87.5 (BC) and 412 (BE) μm . (b),(c) Current-voltage characteristics and bolometer response of $B \parallel E$ [(b), color coded], B [(c), red], and $B-E$ [(c), cyan]. Solid and open triangles in the right panel of (b),(c) point to the first maximum and the second maximum in radiation intensity mentioned in the text, respectively.

A similar I - V - E plot for the CCB of B and E ($B-E$) is shown in Fig. 1(c) together with a plot for B solo. The IVC for $B-E$ below 1 V almost coincides with the IVC

TABLE I. Measured properties for radiations from B , C , E , $B \parallel E$, and $B-E$. P_{max} is the maximum detected radiation power represented bolometer response voltage, I_{max} and V_{max} are current and voltage yielding P_{max} , respectively. N is the number of IJJs contributing to the maximum radiation power averaged to a mesa for comparisons. Superconducting transition temperatures T_c 's and mesa widths of individual B , C , and E are also listed.

	B	C	E	$B \parallel E$	$B-E$
P_{max} (mV)	0.418	0.215	0.468	0.737	0.799
I_{max} (mA)	21.9	33.8	21.7	47.3	18.3
V_{max} (V)	0.983	1.01	0.963	0.903	1.899
N	867	796	879	798	815
T_c	78.5	79.3	78.3		
Mesa width (μm)	66.8	68.2	66.1		

for B . This is interpreted that only B contributes to the voltage and a large part of mesa E remains zero voltage because of the considerable difference in the distributions of the maximum Josephson currents of IJJs composing the mesas B and E seen in Fig. 2 in the Appendices. It is also found that the bolometer responses for B and $B-E$ between 15 and 35 mA with increasing current are superposable. This clearly indicates that only B contributes to the emission power. In the same current range, with decreasing current, on the other hand, significant increase in bolometer response of $B-E$ in comparison to the individual B is observed. The maximum emission of $B-E$ is attained at $I = 18$ mA and the second maximum is found at $I = 26$ mA (indicated by solid and open triangles, respectively). These currents are approximately 4 mA lower and higher than the maximum radiating current of the individuals B and E , respectively. The net mesa voltage for $B-E$ at the maximum emission power is $V = 1.89$ V, which is slightly lower than the sum of the bias voltages for the individual emissions.

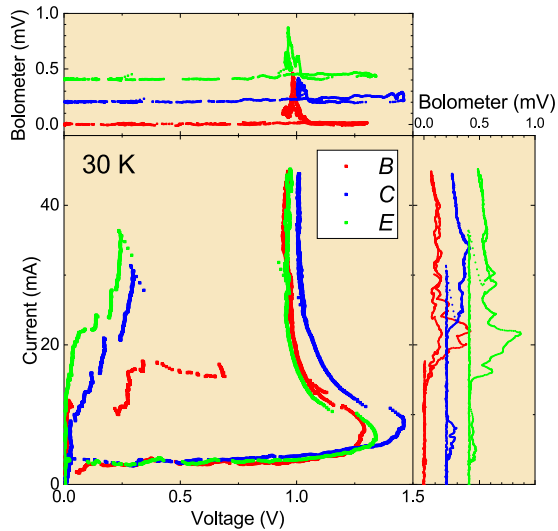


FIG. 2. Current-voltage characteristics (main) and bolometer responses as a function of either current (right) or voltage (upper) for mesas B (red), C (blue), and E (green). The bolometer responses are shifted for clarity. Higher bolometer responses correspond to the case for bias swept down.

These shifts in bias current and voltage have been evaluated theoretically [43]. It is also interesting to note that the bolometer detection in decreasing current of B - E (and B) is not only large but also highly fluctuating in comparison to that in increasing current. This suggests that the coherent radiation is excited in the decreasing current while partly incoherent or chaotic radiation [50,51] may be excited in the increasing current.

B. Spectral characteristics

The radiation spectra of B , C , E , $B \parallel E$, B - E , and B - C are shown in Figs. 3(a) and 3(b). Unimodal spectra are observed not only for individual operations but also for both CVB and CCB, suggesting that multiple mesas are coupled and radiating synchronously. The observed unimodal spectra are as follows: individual (B , 0.43–0.57; C , 0.50–0.55; E , 0.50–0.55 THz), B and E (CVB, 0.47–0.53; CCB, 0.46–0.5 THz), and C and E (CVB, 0.47–0.53; CCB, 0.48–0.61 THz). The frequencies of the emission spectra as functions of the averaged voltage applied to each mesa V_{mesa} are shown in Fig. 3(c). The linear fittings to the plots provide the number, N , of IJJs contributing to the radiations. For the BE pair, in which N 's for individual emissions of B and E are very close approximately 870, and their effective N 's for CVB and CCB radiations are approximately 810, which is 8% smaller than those for B and E individuals. Furthermore, the radiation frequency region of $B \parallel E$ and B - E is close to the overlapping frequency range of B and E , which have slightly shifted radiation frequency range due to the slight difference in mesa width. Thus, the physics of EM radiation of the

mesas B and E under simultaneous bias can be reworded as synchronous oscillations of two oscillators with slightly different eigenfrequencies with a cost of small portion of oscillating Josephson junctions. For simultaneous bias of B and C (CVB, 0.45–0.58; CCB, 0.43–0.55 THz), bimodal spectra are observed, as shown in Fig. 3(b). At this time, the mesas are presumed to be radiating independently. In particular, in the combination of B and C , a unimodal spectrum is observed only at 0.45 THz for CVB, while bimodal spectra are found in the other CVBs and all of the CCBs. The N for C solo is distributed between 780 and 810, which is more than 10% smaller than that for B and E individuals.

The result that CVB operations tend to be coupled is understood as follows. For a CVB, an equal voltage is applied to the two mesas. Although it is not promised to apply an equal voltage to the stacked IJJs composing a mesa structure, the inductive coupling among the IJJs [4] expanding the whole mesa-stack results in an equal voltage being applied because of the Josephson oscillation of an identical frequency. Consequently, an equal voltage is applied to all contributing IJJs, and then Josephson plasma waves of a single frequency are excited in the CVB mesas. The BE and CE pairs, for which a unimodal spectrum is always observed, are presumed to have a relatively strong coupling between the mesas.

It is intriguing that the coupling in the BE pair with larger separation is relatively stronger than that in the combination of the BC pair resulting in synchronous oscillations. The reasons for this are discussed first. The most relevant factor is the commensurability of the intermesa separation d with respect to the mesa width w , which is considered as a dominant factor in the emission frequency of a single mesa. When we consider that the coupling is mediated by the Josephson plasmons, zero-voltage Josephson harmonic oscillations inside the superconducting substrate underneath the mesas, which has been observed as microwave absorption [3,52], the interference between the plasmons and the nonlinear Josephson oscillations excited in the mesas determines the coupling. Here, using $w = 67 \mu\text{m}$ (approximate average of widths of the mesas listed in Table I), d/w values of 1.3 (BC) and 6.1 (BE) are obtained. For combinations with d/w closer to an integer, the effective coupling attributed to the strength of the frequency entrainment of the nonlinear Josephson plasma oscillation is more pronounced. The second most relevant factor is the similarity in the device geometry, including electrodes: mesas B and E are mirror symmetric while C is neither mirror nor translational symmetric with respect to B , and a large overlap in the emission frequency regions of individually biased cases are observed. In other words, for the cases that the device shapes are closer to being equivalent and the emission frequencies are closer, even weak perturbations may cause frequency entrainments, which result in synchronous

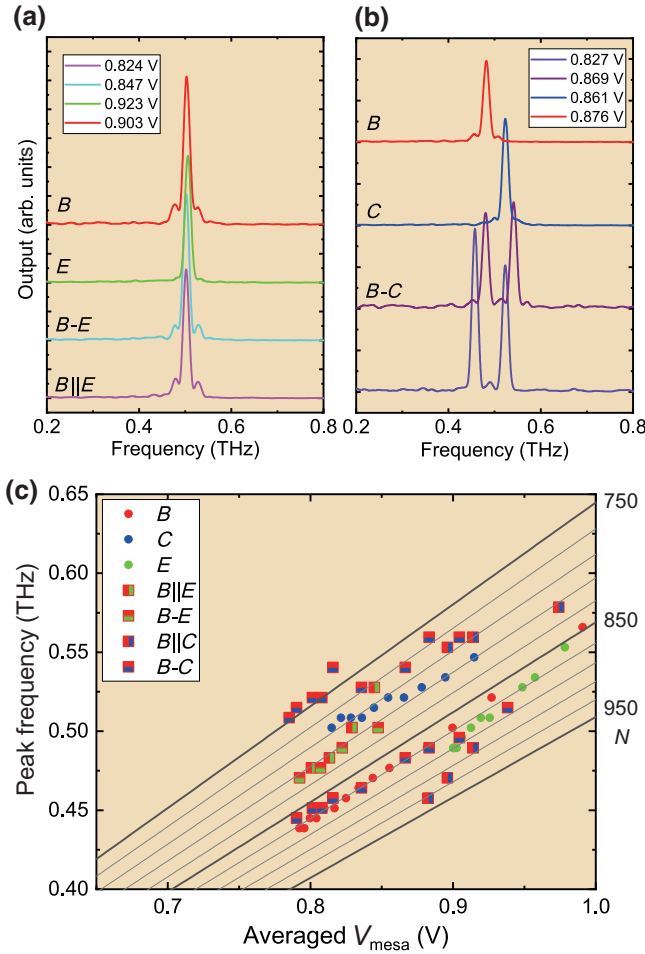


FIG. 3. FTIR spectra of coupled simultaneous radiations (a) and uncoupled simultaneous radiations (b) together with individual radiations at vicinity mesa voltages. In (c), peak frequencies of emission spectra are plotted as functions of averaged mesa voltage V_{mesa} : net voltage divided by 2 for series connections. Thick straight lines mean the ac Josephson relation with corresponding number of IJJs, N . Thin gray lines are drawn for N 's with a step of 20. All data are taken at a bath temperature of 30 K.

radiations. In summary, the BE pair provides coupled phase dynamics between two oscillators with *close eigenfrequencies*.

C. Polarization properties

Next, we discuss polarization on radiations from mesas B , E , and their combinations. Using the polarization analyzer described in Sec. II, we obtain the transmitted intensity as a function of the QWP angle θ for B , E , $B-E$, and $B \parallel E$, as shown in Figs. 4(a) and 4(b). Here, bias voltages to respective mesas are common as 0.92 V, for example. Based on these results, the Stokes polarization parameter SPPs $(S_0, S_1, S_2, S_3) = S_0(1, \tilde{S}_1, \tilde{S}_2, \tilde{S}_3)$ can be estimated by

fitting

$$I(\theta) = \frac{1}{2} (S_0 + S_1 \cos^2 2\theta + S_2 \cos 2\theta \sin 2\theta + S_3 \sin 2\theta), \quad (1)$$

to the experimental data. However, non-negligible twofold asymmetry is found in the experimental data despite the twofold rotationally symmetric function of Eq. (1). This is attributed to an asymmetric loss of the QWP possibly due to deformations of its metallic plates. See Appendix C. In order to reduce this loss, we introduce a correction function $C(\theta)$ as

$$C(\theta) = 1 - \sqrt{a^2 + b^2} + a \cos \theta + b \cos 2\theta, \quad (2)$$

where a and b are constants determined by the optical system. We employ $I_{\text{corr}}(\theta) = C(\theta)I(\theta)$ to apply the least-squares method for the experimental data. This operation corresponds to take a projection to original cross section of intensity from observed results. The obtained SPPs for CVB and CCB are shown in Figs. 4(c) and 4(d), respectively. The values are listed in Table II. Between mesa B and E , no significant difference is found for S_0, \tilde{S}_1 , and \tilde{S}_2 , whereas \tilde{S}_3 has the opposite sign, i.e., opposite helicity. This is attributed to the mirror symmetry of the device shapes including their electrodes. Next, let us compare among individual and simultaneous bias cases. S_0 's for both CVB and CCB cases considerably smaller than the square of the sum of $\sqrt{S_0}$'s for individual cases. Significant difference in \tilde{S}_3 is found between CVB and CCB. This is attributed to the phase delay to synchronize B and E .

1. Linear combination method to describe a coupled emission

Let us consider the coupled radiation of the BE pair. If we write electric field emitted from the individually biased mesas B and E as $|B\rangle = \mathbf{E}_B \exp[i(\omega_B t + \delta_B)]$ and $|E\rangle = \mathbf{E}_E \exp[i(\omega_E t + \delta_E)]$, respectively, where \mathbf{E}_B , ω_B , and δ_B are the electric field vector, angular frequency, and the phase of an EM wave emitted from mesa B , respectively. The simultaneous bias in the parallel connection can be written as follows:

$$|B \parallel E\rangle = \alpha |B\rangle + \beta |E\rangle, \quad (3)$$

where α and β are complex. This is based on the idea that the observed coupled emission $|B \parallel E\rangle$ is a superposition of the EM waves emitted from mesas B and E under CVB, referred to as $|B'\rangle$ and $|E'\rangle$, which are results of perturbation arising from the coupling interaction $V_{B \parallel E}$ to $|B\rangle$ and

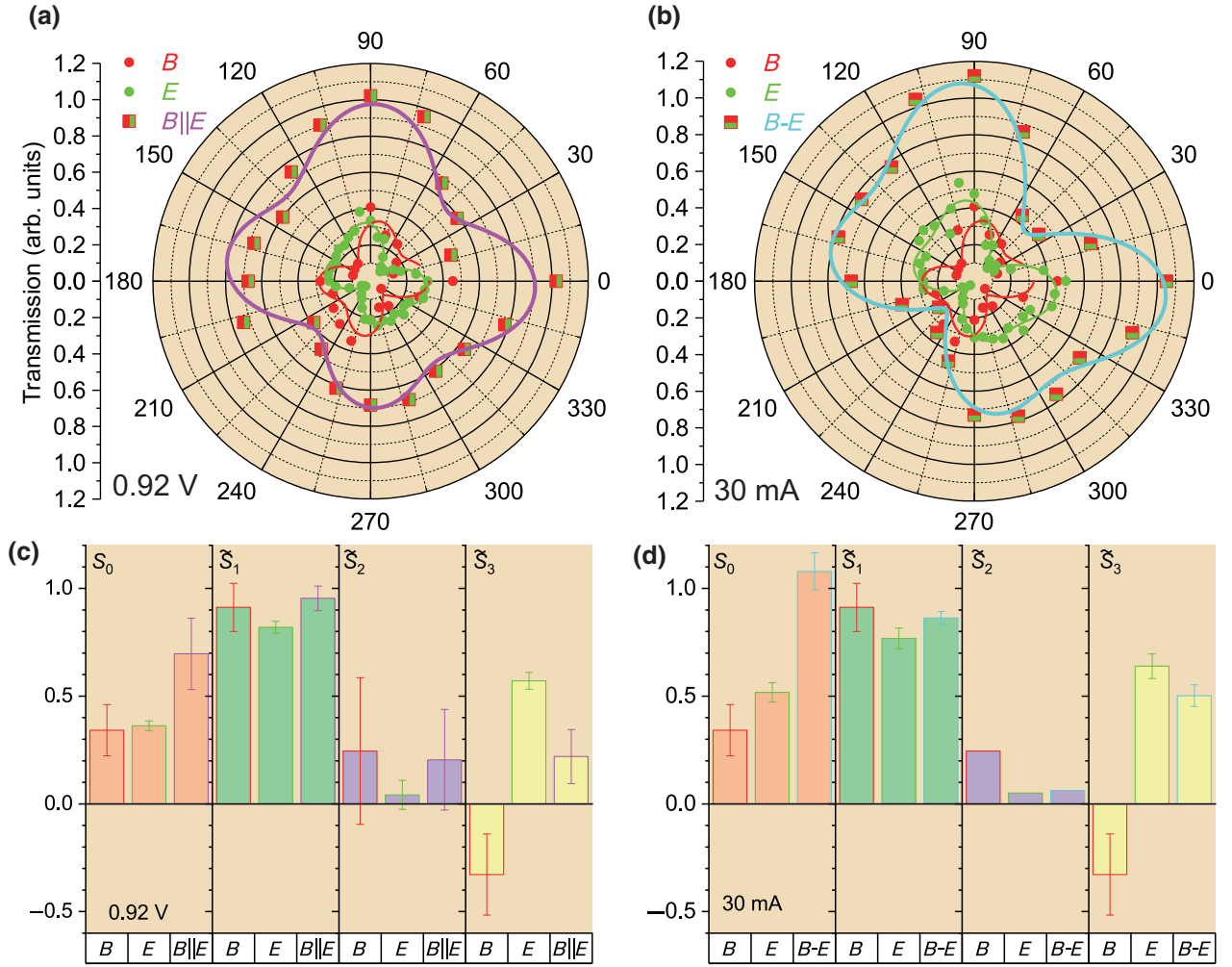


FIG. 4. (a),(b) Polar plots of transmission intensity of B , E , $B \parallel E$ (a), and $B-E$ (b) through the polarization analyzer. Data at 0.92 V and 30 mA are plotted in (a),(b), respectively. Symbols represent measured intensity and curves are least-squares fitting results of $I_{\text{corr}}(\theta)$ given by Eqs. (1) and (2) to derive SPPs. (c),(d) Derived SPPs from (a),(b) are shown in (c),(d), respectively. S_0 , \tilde{S}_1 , and \tilde{S}_2 show no significant difference among B , E , $B \parallel E$ and $B-E$. \tilde{S}_3 representing helicity of EM vector has opposite sign between B and E . This is due to the mirror symmetry of the device shape between them.

$|E\rangle$, respectively. Thus,

$$\begin{pmatrix} |B'\rangle \\ |E'\rangle \end{pmatrix} = V_{B\parallel E} \begin{pmatrix} |B\rangle \\ |E\rangle \end{pmatrix} = \begin{pmatrix} \alpha_1 & \beta_1 \\ \alpha_2 & \beta_2 \end{pmatrix} \begin{pmatrix} |B\rangle \\ |E\rangle \end{pmatrix}, \quad (4)$$

where $\alpha = \alpha_1 + \alpha_2$ and $\beta = \beta_1 + \beta_2$ [36]. Writing $|B \parallel E\rangle = \mathbf{E}_{B\parallel E} \exp[i(\omega_{B\parallel E}t + \delta_{B\parallel E})]$, we obtain $\alpha(\omega_B) = |\alpha| \exp[i(\omega'_B t + \delta'_B)]$ and $\beta(\omega_E) = |\beta| \exp[i(\omega'_E t + \delta'_E)]$ with $\omega_{B\parallel E} = \omega_B + \omega'_B = \omega_E + \omega'_E$ and $\delta_{B\parallel E} = \delta_B + \delta'_B = \delta_E + \delta'_E$. Here, ω'_B and δ'_B are the frequencies and phase changes of mesa B associated with synchronization, which indicates the magnitude of the intermesa perturbation. It is considered that $|\alpha|$ and $|\beta|$ correspond to the ratios of the number of IJJs contributing to for the coupled emission (N'_B and N'_E) with respect to those for the individual emissions (N_B and N_E); in other words, $|\alpha| = N'_B/N_B$

and etc. $\delta_\gamma = \arg(\beta/\alpha) = \delta'_E - \delta'_B$ is the phase difference of the coupling perturbation for mesas B and E , which may relate to the separation between the two mesas and the wavelength of the simultaneous oscillations of the two mesas. In the following, we derive

$$(\alpha, \beta) = |BE\rangle \begin{pmatrix} |B\rangle \\ |E\rangle \end{pmatrix}^{-1}, \quad (5)$$

where $|BE\rangle$ is either $|B \parallel E\rangle$ or $|B-E\rangle$, and the validity of determining α and β is discussed with fixing bases as specific polarizations of individual emissions in the following section.

TABLE II. Derived Stokes polarization parameters at given individual and simultaneous bias conditions.

	Bias	S_0	\tilde{S}_1	\tilde{S}_2	\tilde{S}_3
B	0.918 V	0.341	0.912	0.245	-0.328
E	0.917 V	0.362	0.819	0.041	0.571
$B \parallel E$	0.921 V	0.696	0.953	0.204	0.219
B	0.974 V	0.530	0.728	0.513	-0.453
E	0.984 V	0.471	0.722	-0.104	0.683
$B \parallel E$	0.974 V	0.528	0.699	-0.167	0.694
B	30 mA	0.341	0.912	0.245	-0.328
E	30 mA	0.517	0.767	0.050	0.638
$B-E$	30 mA	1.079	0.862	0.062	0.501

2. Fixed bias analysis results and discussion

First, let us discuss synchronization between two mesas in CVB mode. Since an equal voltage is applied for both mesas in the CVB mode, two sets of SPPs of $|B\rangle$, $|E\rangle$, and $|B \parallel E\rangle$ at two constant voltages are employed and compare their coefficients α and β derived by Eq. (5). Here, we assume that the oscillation frequency of the mesa does not change accompanied by the synchronization, i.e., $\omega'_B = \omega'_E = 0$. The coefficients for $V_{\text{mesa}} = 0.92$ and 0.97 V are listed in Table III. The set of (α, β) at 0.92 V shows that the most of IJJs in both mesas B and E contribute to the radiation with 20° phase difference. Here, the Josephson oscillation in the mesas B and E are apparently synchronized. On the other hand, at $V_{\text{mesa}} = 0.97$ V, the obtained coefficients imply that only a small portion of IJJs composing the mesa B participates in the radiation for $B \parallel E$. Here, the phase difference δ_γ does not make sense. This would be attributed to larger deviation in radiation frequency of $B \parallel E$ from individual B . As an example of CCB mode, we discuss $I_{\text{mesa}} = 30$ mA, shown in Figs. 4(b) and 4(d). The obtained $|\alpha|$ is less than 0.3, suggesting that only 30% of IJJs of mesa B participates in the synchronization. This seems to be consistent with the spectroscopic analysis that the CCB mode tends to show a bimodal FTIR spectrum.

In our previous publications [36,37], the bases used for the linear combination analysis were regarded as the polarizations with the intensity maxima of individual bias operations. A polarization of parallelly connected mesas was composed from two polarizations of single mesas at biases determined by radiation properties of respectively specified conditions. This procedure is considered

TABLE III. Obtained linear-coupling coefficients α, β , and $\delta_\gamma = \arg(\beta/\alpha)$.

	Bias	$ \alpha $	$ \beta $	δ_γ (deg)
(a)	$B \parallel E$ 0.92 V	0.632	0.824	17.4
(b)	$B \parallel E$ 0.97 V	0.145	0.953	306.1
(c)	$B-E$ 30 mA	0.297	1.23	-9.02

to be the same as previous works for synchronous radiations of multiple mesas, where intensities and spectra at biases selected by their authors with implicit aspects are compared to discuss correspondences between individual and simultaneous bias operations [34,35]. However, the requirement of common voltage or current either for parallel or series connection has not been necessarily taken into considerations.

Our analysis relies on three specific measured polarizations: a coupled emission with respect to two individual emissions. Considering the known facts on JPE, i.e., that emission intensity and polarization are sensitive to the temperature distribution of the device [22], it is natural to presume that the temperature distribution of the simultaneous emission is different from the individual emissions. This discrepancy may result in deviations of $|\alpha|$ and $|\beta|$ from unity. Let us apply these bases to the neighboring

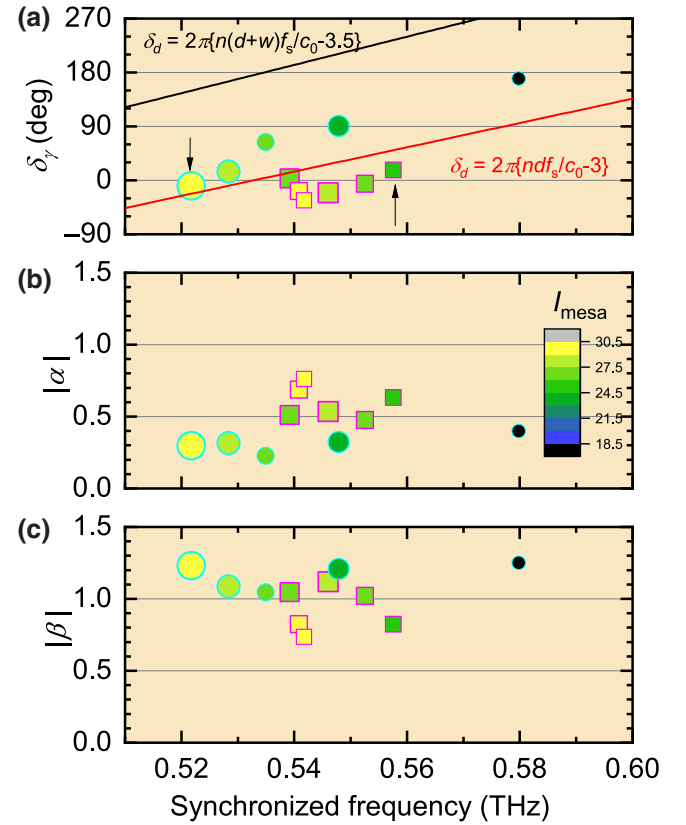


FIG. 5. Estimated phase delay δ_γ (a), $|\alpha|$ (b), and $|\beta|$ (c) between the synchronized mesas as a function of synchronized frequency f_s for CVB (square) and CCB (circle) operations. Symbol size represents scaled S_0 and colors represent averaged bias current I_{mesa} for the synchronized radiation. Solid lines are phase difference corresponding to the mesa separation d and mesa pitch $d + w$ of traveling waves inside a media with a refractive index $n = 4.2$. Arrows in (a) point out data without frequency shift between individual and synchronized radiations, which are listed at rows (a),(c) of Table III.

synchronous radiations to find frequency evolutions of the phase shift δ_γ . Here, the frequency shift due to the mesa interaction ω' is explicit. Figure 5 shows δ_γ , $|\alpha|$, and $|\beta|$ as functions of synchronized frequency f_s for CVB radiations with bases at 0.92 V used in the previous paragraphs. Obtained parameters for CCB radiations with bases at 30 mA is also plotted. It is found that the phase shift varies linearly with increasing frequency as the general trend common for CVB and CCB. The expected phase shift from the separation between the mesas $\delta_d = 2\pi n d f_s / c_0$ is drawn with a solid line. Noted that δ_γ obtained with using 0.97-V bases shows no consistent trend. For CCB, the evolution also follows to δ_d but the phase offset is different from CVB. The common slope in the frequency evolution of δ_γ close to δ_d determined by the refractive index of the superconducting substrate $n \simeq 4.2$ [17] suggests that the interaction between the mesas are mediated not by electromagnetic waves in the space but by plasmons inside the Bi2212 single crystal. An expected phase delay in accordance of the *pitch* of the mesas $\delta_{d+w} = 2\pi n(d+w)f_s/c_0$ is also plotted in Fig. 5(a). The agreement to the experimental δ_γ looks less likely than the case of δ_d , however further analyses on synchronized radiations among closer mesas (smaller d/w ; C and D for the present device) are required to judge the dominant distance factor (d or $d+w$) for synchronized oscillation between mesas.

The systematic difference between CVB and CCB observed in the present study presents quantitative differences of media to promote the synchronous radiation; in other words, the Josephson plasmon excited the base crystal. To attain the highest radiation power accompanied by fully controlled in-phase synchronization, δ_γ holds an essential relevance for CVB, and the number of synchronously oscillating IJJs within a mesa is another relevance for CCB. In Ref. [38], it is reported that the phase delay between two synchronized IJJ stacks composing the same number of IJJs is zero. The difference from the present study may be attributed to the small difference in N , individual radiation frequency, inhomogeneous temperature rise, and so on. These inevitable inequivalences of a real device can be compensated by an externally applied perturbation such as an external magnetic field or a focused laser irradiation. We believe that the suggested polarimetry under the controlled perturbations and numerical analysis on Josephson junctions with modified coupling capacitances [53] elucidate the mechanism for coherent phase dynamics of a Josephson-junction array. Furthermore, investigations on CVB and CCB systems with more mesas in combination with artificially fabricated Josephson-junction arrays [54] leads to multipixel two-dimensional JPE mesa array devices and a global coupling system of Josephson oscillators [55], which represents synchronous phenomena within a mesa consisting of thousands of IJJs.

IV. SUMMARY

Terahertz electromagnetic wave emission from two simultaneously biased mesas of Bi2212 IJJ stacks on a superconducting substrate is investigated by intensity, frequency, and polarization measurements as functions of bias voltage, combination of mesas, and parallel and series connections. Coupled and uncoupled emissions tended to be observed in parallel and series connections of the mesas, respectively. The frequencies of the coupled emissions are systematically varied. Electromagnetic waves from pairs of coupled mesas can be represented by linear combinations of two individual emissions at shifted frequencies and phases, irrespective of parallel and series connections, rather than by simple superpositions of observed individual radiations modified by device temperature rise. Further systematic investigations with parameters of intermesa separation and mesa geometries are required to fully assess the features of the perturbation matrix to control the intermesa synchronous phenomena and attain a high-power terahertz source from superconducting IJJ stacks.

ACKNOWLEDGMENTS

This work is supported by the Japan Society for the Promotion of Science (JSPS) KAKENHI (Grant No. JP20H02606) and JSPS—Centre national de la recherche scientifique (CNRS) Bilateral Program (Grant No. JSPSPB120192908).

APPENDIX A: BASIC PROPERTIES OF INDIVIDUAL MESAS

Geometries, superconducting transition temperature T_c characterizing mesas B , C , and E are listed in Table I. The length and thickness of the mesas are designed to be the same as 350 and 80 μm . Figure 2 shows current-voltage-emission I - V - E characteristics for mesas B , C , and E . Dominant high-bias radiation and weak low-bias radiation are found [24]. The high-bias radiation is found in all mesas and the low-bias radiation is found in mesas C and E . The high-bias radiation is pronounced below 35, 25, and 45 K for mesas B , C , E , respectively. Thus, discussion to compare individual and simultaneous emissions is done for data acquired at 30 K.

Temperature dependence of the radiation intensity for individual biasing are shown in Fig. 6. The intensity maxima in B and E are found at 30 and 36 K, respectively. Comparing the intensity at 30 K, where simultaneous bias data are taken, with the data at higher temperatures, E can increase by more than 10% with a temperature rise of about 6 K, but B decreases by more than that, so that the sum of intensities is smaller than that at 30 K. For these reasons, we can conclude that the radiation intensity in simultaneous bias is not due to the temperature increase added to the superposition of the individual radiations.

APPENDIX B: POLARIZATION DATA ACQUISITION

The voltage-current dependences of SPPs are extracted from I - V - E curves at varied QWP angle θ of the system shown in Ref. [36]. First, we obtain I - V - E data at every fixed θ for several I - V rounds, where θ is changed from 0 to 360° with a step of 9 or 18° . Second, a polar plot of the transmission intensities is made to pick up E values within a certain I - V window (e.g., $1 \text{ mA} \times 0.05 \text{ V}$) for θ s. Here, E -data points, which apparently deviates from the twofold rotational (C2) symmetry are removed. Then, SPPs are obtained by fitting Eq. (1) to the polar plot. The obtained values compose SPPs at the bias of the center of the I - V window.

For comparisons among different mesas and different connections, normalized SPPs ($1, \tilde{S}_1, \tilde{S}_2, \tilde{S}_3$), where $\tilde{S}_i = S_i/S_0$ ($i = 1, 2, 3$) are useful. Values of obtained SPPs used to estimate α and β according to Sec. III C 1 are listed in Table II.

APPENDIX C: CORRECTION FUNCTION FOR TWOFOLD ASYMMETRY

Since the QWP used in this work consists of thin metallic plates held by a pair of pillars [46], a possible local deformation of the plates results in asymmetric transmission through the QWP. This is pronounced when the THz beam is not centered at the QWP. To obtain reliable SPPs, we introduce a correction function $C(\theta)$, Eq. (2). $C(\theta)$ is found from 2π periodic functions with respect to θ to restore the loss of QWP due to the deformation. Thus $\max_{0 \leq \theta < 2\pi} \{C(\theta)\} = 1$ is satisfied as shown in Fig. 7.

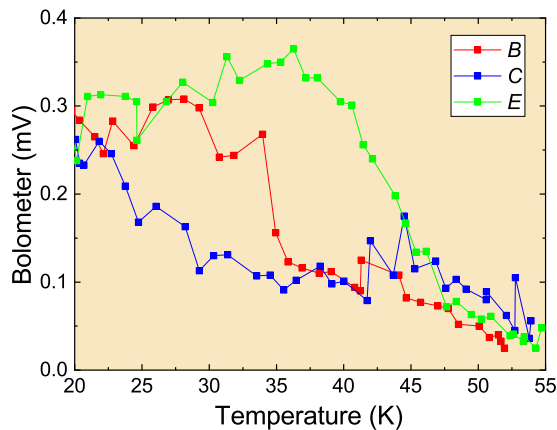


FIG. 6. Temperature dependence of the maximum radiation intensity for individual B , C , and E .

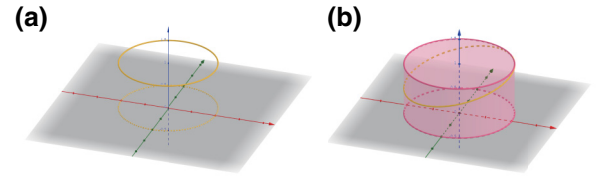


FIG. 7. Schematic representations of the correction function $C(\theta)$. (a) Homogeneous loss case with $C(\theta) = 1$. (b) Assume that the observed transmission intensity is a result of a linearly dependent spatial loss (of the QWP). Observed intensity corresponds to the red circle with respect to real incident intensity represented by the yellow ellipse with $C(\theta) = 1 + 0.25 \sin(\theta + 1) - 0.25$.

APPENDIX D: TRANSFORMATION FROM STOKES POLARIZATION PARAMETERS TO ELECTRIC VECTOR

Consider a completely polarized electromagnetic wave whose electric field in the plane perpendicular to the propagation vector given by

$$\mathbf{E}(t) = \begin{pmatrix} E_x \exp[i\omega t] \\ E_y \exp[i(\omega t + \delta_{xy})] \end{pmatrix}, \quad (\text{D1})$$

where the observation plane is taken at $z = 0$ and ω is the angular frequency of the wave. The polarization of this electromagnetic wave is represented by a set of SPPs

$$\begin{pmatrix} S_0 \\ S_1 \\ S_2 \\ S_3 \end{pmatrix} = \begin{pmatrix} E_x^2 + E_y^2 \\ E_x^2 - E_y^2 \\ 2E_x E_y \cos \delta_{xy} \\ 2E_x E_y \sin \delta_{xy} \end{pmatrix}. \quad (\text{D2})$$

The parameters of the electric field is oppositely obtained by the SPPs as

$$\begin{aligned} E_x &= \sqrt{\frac{S_0 + S_1}{2}} \\ E_y &= \sqrt{\frac{S_0 - S_1}{2}}, \\ \delta_{xy} &= \arctan \frac{S_3}{S_2} \end{aligned} \quad (\text{D3})$$

which are used to obtain complex coefficients of α and β with Eq. (5).

- [1] R. Kleiner, F. Steinmeyer, G. Kunkel, and P. Müller, Intrinsic Josephson Effects in $\text{Bi}_2\text{Sr}_2\text{CaCu}_2\text{O}_8$ Single Crystals, *Phys. Rev. Lett.* **68**, 2394 (1992).
- [2] M. Tachiki, T. Koyama, and S. Takahashi, Electromagnetic phenomena related to a low-frequency plasma in cuprate superconductors, *Phys. Rev. B* **50**, 7065 (1994).

- [3] I. Takeya, K. Kindo, K. Kadowaki, S. Takahashi, and T. Mochiku, Mode separation of the Josephson plasma in $\text{Bi}_2\text{Sr}_2\text{CaCu}_2\text{O}_{8+\delta}$, *Phys. Rev. B* **57**, 3108 (1998).
- [4] S. Sakai, P. Bodin, and N. F. Pedersen, Fluxons in thin-film superconductor-insulator superlattices, *J. Appl. Phys.* **73**, 2411 (1993).
- [5] T. Koyama and M. Tachiki, I - V characteristics of Josephson-coupled layered superconductors with longitudinal plasma excitations, *Phys. Rev. B* **54**, 16183 (1996).
- [6] M. Machida, T. Koyama, and M. Tachiki, Dynamical Breaking of Charge Neutrality in Intrinsic Josephson Junctions: Common Origin for Microwave Resonant Absorptions and Multiple-Branch Structures in the I - V Characteristics, *Phys. Rev. Lett.* **83**, 4618 (1999).
- [7] M. Machida and S. Sakai, Unified theory for magnetic and electric field coupling in multistacked Josephson junctions, *Phys. Rev. B* **70**, 144520 (2004).
- [8] M. Machida, T. Koyama, A. Tanaka, and M. Tachiki, Collective dynamics of Josephson vortices in intrinsic Josephson junctions: Exploration of in-phase locked superradiant vortex flow states, *Phys. C Supercond. its Appl.* **330**, 85 (2000).
- [9] M. Tachiki, M. Iizuka, K. Minami, S. Tejima, and H. Nakamura, Emission of continuous coherent terahertz waves with tunable frequency by intrinsic Josephson junctions, *Phys. Rev. B - Condens. Matter Mater. Phys.* **71**, 134515 (2005).
- [10] L. N. Bulaevskii and A. E. Koshelev, Radiation due to Josephson Oscillations in Layered Superconductors, *Phys. Rev. Lett.* **99**, 057002 (2007).
- [11] L. Ozyuzer, A. E. Koshelev, C. Kurter, N. Gopalsami, Q. Li, M. Tachiki, K. Kadowaki, T. Yamamoto, H. Minami, H. Yamaguchi, T. Tachiki, K. E. Gray, W.-K. Kwok, and U. Welp, Emission of coherent THz radiation from superconductors, *Science* **318**, 1291 (2007).
- [12] K. Kadowaki, H. Yamaguchi, K. Kawamata, T. Yamamoto, H. Minami, I. Takeya, U. Welp, L. Ozyuzer, A. Koshelev, C. Kurter, K. E. Gray, and W. K. Kwok, Direct observation of terahertz electromagnetic waves emitted from intrinsic Josephson junctions in single crystalline $\text{Bi}_2\text{Sr}_2\text{CaCu}_2\text{O}_{8+\delta}$, *Phys. C Supercond. its Appl.* **468**, 634 (2008).
- [13] H. Minami, I. Takeya, H. Yamaguchi, T. Yamamoto, and K. Kadowaki, Characteristics of terahertz radiation emitted from the intrinsic Josephson junctions in high- T_c superconductor $\text{Bi}_2\text{Sr}_2\text{CaCu}_2\text{O}_{8+\delta}$, *Appl. Phys. Lett.* **95**, 232511 (2009).
- [14] X. Hu and S.-Z. Lin, Phase dynamics in a stack of inductively coupled intrinsic Josephson junctions and terahertz electromagnetic radiation, *Supercond. Sci. Technol.* **23**, 053001 (2010).
- [15] H. B. Wang, S. Guénon, B. Gross, J. Yuan, Z. G. Jiang, Y. Y. Zhong, M. Grünzweig, A. Iishi, P. H. Wu, T. Hatano, D. Koelle, and R. Kleiner, Coherent Terahertz Emission of Intrinsic Josephson Junction Stacks in the Hot Spot Regime, *Phys. Rev. Lett.* **105**, 057002 (2010).
- [16] A. Yurgens, Temperature distribution in a large $\text{Bi}_2\text{Sr}_2\text{CaCu}_2\text{O}_{8+\delta}$ mesa, *Phys. Rev. B* **83**, 184501 (2011).
- [17] T. Kashiwagi, K. Yamaki, M. Tsujimoto, K. Deguchi, N. Orita, T. Koike, R. Nakayama, H. Minami, T. Yamamoto, R. a. Klemm, M. Tachiki, and K. Kadowaki, Geometrical full-wavelength resonance mode generating terahertz waves from a single-crystalline $\text{Bi}_2\text{Sr}_2\text{CaCu}_2\text{O}_{8+\delta}$ rectangular mesa, *J. Phys. Soc. Jpn.* **80**, 094709 (2011).
- [18] T. Koyama, H. Matsumoto, M. Machida, and Y. Ota, Multi-scale simulation for terahertz wave emission from the intrinsic Josephson junctions, *Supercond. Sci. Technol.* **24**, 085007 (2011).
- [19] I. Takeya, Y. Omukai, T. Yamamoto, K. Kadowaki, and M. Suzuki, Effect of thermal inhomogeneity for terahertz radiation from intrinsic Josephson junction stacks of $\text{Bi}_2\text{Sr}_2\text{CaCu}_2\text{O}_{8+\delta}$, *Appl. Phys. Lett.* **100**, 242603 (2012).
- [20] U. Welp, K. Kadowaki, and R. Kleiner, Superconducting emitters of THz radiation, *Nat. Photonics* **7**, 702 (2013).
- [21] M. Li, J. Yuan, N. Kinev, J. Li, B. Gross, S. Guénon, A. Ishii, K. Hirata, T. Hatano, D. Koelle, R. Kleiner, V. P. Koshelets, H. Wang, and P. Wu, Linewidth dependence of coherent terahertz emission from $\text{Bi}_2\text{Sr}_2\text{CaCu}_2\text{O}_8$, *Phys. Rev. B* **86**, 060505(R) (2012).
- [22] M. Tsujimoto, H. Kambara, Y. Maeda, Y. Yoshioka, Y. Nakagawa, and I. Takeya, Dynamic Control of Temperature Distributions in Stacks of Intrinsic Josephson Junctions in $\text{Bi}_2\text{Sr}_2\text{CaCu}_2\text{O}_{8+\delta}$, *Phys. Rev. Appl.* **2**, 044016 (2014).
- [23] L. Y. Hao, *et al.*, Compact Superconducting Terahertz Source Operating in Liquid Nitrogen, *Phys. Rev. Appl.* **3**, 024006 (2015).
- [24] I. Takeya and H. Wang, Terahertz-wave emission from $\text{Bi}2212$ intrinsic Josephson junctions: a review on recent progress, *Supercond. Sci. Technol.* **29**, 073001 (2016).
- [25] T. Kashiwagi, H. Kubo, K. Sakamoto, T. Yuasa, Y. Tanabe, C. Watanabe, T. Tanaka, Y. Komori, R. Ota, G. Kuwano, K. Nakamura, T. Katsuragawa, M. Tsujimoto, T. Yamamoto, R. Yoshizaki, H. Minami, K. Kadowaki, and R. A. Klemm, The present status of high- T_c superconducting terahertz emitters, *Supercond. Sci. Technol.* **30**, 074008 (2017).
- [26] E. A. Borodianskyi and V. M. Krasnov, Josephson emission with frequency span 1–11 THz from small $\text{Bi}_2\text{Sr}_2\text{CaCu}_2\text{O}_{8+\delta}$ mesa structures, *Nat. Commun.* **8**, 1742 (2017).
- [27] A. Elarabi, Y. Yoshioka, M. Tsujimoto, and I. Takeya, Monolithic Superconducting Emitter of Tunable Circularly Polarized Terahertz Radiation, *Phys. Rev. Appl.* **8**, 064034 (2017).
- [28] A. Elarabi, Y. Yoshioka, M. Tsujimoto, and I. Takeya, Circularly polarized terahertz radiation monolithically generated by cylindrical mesas of intrinsic Josephson junctions, *Appl. Phys. Lett.* **113**, 052601 (2018).
- [29] R. Kleiner and H. Wang, Terahertz emission from $\text{Bi}_2\text{Sr}_2\text{CaCu}_2\text{O}_{8+x}$ intrinsic Josephson junction stacks, *J. Appl. Phys.* **126**, 171101 (2019).
- [30] T. M. Benseman, A. E. Koshelev, V. Vlasko-Vlasov, Y. Hao, U. Welp, W.-K. Kwok, B. Gross, M. Lange, D. Koelle, R. Kleiner, H. Minami, M. Tsujimoto, and K. Kadowaki, Observation of a two-mode resonant state in a $\text{Bi}_2\text{Sr}_2\text{CaCu}_2\text{O}_{8+\delta}$ mesa device for terahertz emission, *Phys. Rev. B* **100**, 144503 (2019).
- [31] G. Kuwano, M. Tsujimoto, Y. Kaneko, T. Imai, Y. Ono, S. Nakagawa, S. Kusunose, H. Minami, T. Kashiwagi, K.

- Kadowaki, Y. Simsek, U. Welp, and W.-K. Kwok, Mesa-Sidewall Effect on Coherent Terahertz Radiation via Spontaneous Synchronization of Intrinsic Josephson Junctions in $\text{Bi}_2\text{Sr}_2\text{CaCu}_2\text{O}_{8+\delta}$, *Phys. Rev. Appl.* **13**, 014035 (2020).
- [32] Y. Ono, H. Minami, G. Kuwano, T. Kashiwagi, M. Tsujimoto, K. Kadowaki, and R. A. Klemm, Superconducting Emitter Powered at 1.5 Terahertz by an External Resonator, *Phys. Rev. Appl.* **13**, 064026 (2020).
- [33] Y. Saito, S. Adachi, R. Matsumoto, M. Nagao, S. Fujita, K. Hayama, K. Terashima, H. Takeya, I. Kakeya, and Y. Takano, THz emission from a $\text{Bi}_2\text{Sr}_2\text{CaCu}_2\text{O}_{8+\delta}$ cross-whisker junction, *Appl. Phys. Express* **14**, 033003 (2021).
- [34] N. Orita, H. Minami, T. Koike, T. Yamamoto, and K. Kadowaki, Synchronized operation of two serially connected $\text{Bi}2212$ THz emitters, *Phys. C Supercond. its Appl.* **470**, S786 (2010).
- [35] T. M. Benseman, K. E. Gray, a. E. Koshelev, W.-K. Kwok, U. Welp, H. Minami, K. Kadowaki, and T. Yamamoto, Powerful terahertz emission from $\text{Bi}_2\text{Sr}_2\text{CaCu}_2\text{O}_{8+\delta}$ mesa arrays, *Appl. Phys. Lett.* **103**, 022602 (2013).
- [36] M. Tsujimoto, S. Fujita, G. Kuwano, K. Maeda, A. Elarabi, J. Hawecker, J. Tignon, J. Mangeney, S. Dhillion, and I. Kakeya, Mutually Synchronized Macroscopic Josephson Oscillations Demonstrated by Polarization Analysis of Superconducting Terahertz Emitters, *Phys. Rev. Appl.* **13**, L051001 (2020).
- [37] K. Hayama, S. Fujita, Y. Kuriyama, K. Maeda, M. Tsujimoto, and I. Kakeya, in *2020 Int. Conf. UK-China Emerg. Technol.* (IEEE, 2020), p. 1.
- [38] S.-Z. Lin, Mutual synchronization of two stacks of intrinsic Josephson junctions in cuprate superconductors, *J. Appl. Phys.* **115**, 173901 (2014).
- [39] K. Ota, K. Hamada, R. Takemura, M. Ohmaki, T. Machi, K. Tanabe, M. Suzuki, A. Maeda, and H. Kitano, Comparative study of macroscopic quantum tunneling in $\text{Bi}_2\text{Sr}_2\text{CaCu}_2\text{O}_y$, *Phys. Rev. B* **79**, 134505 (2009).
- [40] H. Kitano, Y. Takahashi, D. Kakehi, H. Yamaguchi, S.-i. Koizumi, and S.-y. Ayukawa, Increase of phase retrapping effects in the switching rate from the finite voltage state of the underdamped intrinsic Josephson junctions, *J. Phys. Soc. Jpn.* **85**, 054703 (2016).
- [41] Y. Nomura, T. Mizuno, H. Kambara, Y. Nakagawa, and I. Kakeya, Enhanced macroscopic quantum tunneling in capacitively coupled $\text{BiPb}2201$ single-layered intrinsic Josephson junctions, *J. Phys. Soc. Jpn.* **84**, 013704 (2015).
- [42] Y. Nomura, R. Okamoto, T.-a. Mizuno, S. Adachi, T. Watanabe, M. Suzuki, and I. Kakeya, Role of the inner copper oxide plane in interlayer Josephson effects in multilayered cuprate superconductors, *Phys. Rev. B* **100**, 144515 (2019).
- [43] S.-Z. Lin and A. E. Koshelev, Synchronization of Josephson oscillations in a mesa array of $\text{Bi}_2\text{Sr}_2\text{CaCu}_2\text{O}_{8+\delta}$ through the Josephson plasma waves in the base crystal, *Phys. C Supercond.* **491**, 24 (2013).
- [44] H. Eisele, M. Naftaly, and J. R. Fletcher, A simple interferometer for the characterization of sources at terahertz frequencies, *Meas. Sci. Technol.* **18**, 2623 (2007).
- [45] I. Kakeya, N. Hirayama, T. Nakagawa, Y. Omukai, and M. Suzuki, Temperature and current dependencies of terahertz emission from stacks of intrinsic Josephson junctions with thin electrodes revealed by a high-resolution FT-IR spectrometer, *Phys. C Supercond.* **491**, 11 (2013).
- [46] M. Nagai, N. Mukai, Y. Minowa, M. Ashida, T. Suzuki, J. Takayanagi, and H. Ohtake, Achromatic wave plate in THz frequency region based on parallel metal plate waveguides with a pillar array, *Opt. Express* **23**, 4641 (2015).
- [47] B. Schaefer, E. Collett, R. Smyth, D. Barrett, and B. Fraher, Measuring the Stokes polarization parameters, *Am. J. Phys.* **75**, 163 (2007).
- [48] G. Y. Russell A. Chipman and Wai-Sze Tiffany Lam, *Polarized Light and Optical Systems* (CRC Press, Boca Raton, 2019), 251.
- [49] B. Gross, F. Rudau, N. Kinev, M. Tsujimoto, J. Yuan, Y. Huang, M. Ji, X. J. Zhou, D. Y. An, a. Ishii, P. H. Wu, T. Hatano, D. Koelle, H. B. Wang, V. P. Koshelets, and R. Kleiner, Electrothermal behavior and terahertz emission properties of a planar array of two $\text{Bi}_2\text{Sr}_2\text{CaCu}_2\text{O}_{8+\delta}$ intrinsic Josephson junction stacks, *Supercond. Sci. Technol.* **28**, 055004 (2015).
- [50] D. R. Gulevich, V. P. Koshelets, and F. V. Kusmartsev, Bridging the terahertz gap for chaotic sources with superconducting junctions, *Phys. Rev. B* **99**, 060501(R) (2019).
- [51] E. M. Shahverdiev, Modulated time delays, synchronized Josephson junctions in high-temperature superconductors and chaotic terahertz waves, *J. Supercond. Nov. Magn.* **34**, 1125 (2021).
- [52] Y. Matsuda, M. Gaifullin, K. Kumagai, K. Kadowaki, and T. Mochiku, Collective Josephson Plasma Resonance in the Vortex State of $\text{Bi}_2\text{Sr}_2\text{CaCu}_2\text{O}_{8+\delta}$, *Phys. Rev. Lett.* **75**, 4512 (1995).
- [53] I. Ottaviani, M. Cirillo, M. Lucci, V. Merlo, M. Salvato, M. G. Castellano, G. Torrioli, F. Mueller, and T. Weimann, Collective cavity mode excitations in arrays of Josephson junctions, *Phys. Rev. B* **80**, 174518 (2009).
- [54] M. Galin, F. Rudau, E. Borodianskyi, V. Kurin, D. Koelle, R. Kleiner, V. Krasnov, and A. Klushin, Direct Visualization of Phase-Locking of Large Josephson Junction Arrays by Surface Electromagnetic Waves, *Phys. Rev. Appl.* **14**, 024051 (2020).
- [55] K. Wiesenfeld, P. Colet, and S. Strogatz, Frequency locking in Josephson arrays: Connection with the Kuramoto model, *Phys. Rev. E* **57**, 1563 (1998).